European Polymer Journal 84 (2016) 300–312

Contents lists available at ScienceDirect

European Polymer Journal

journal homepage: www.elsevier.com/locate/europolj

High-performance and multifunctional epoxy composites filled with epoxide-functionalized graphene

Shuai Zhao, Haiyan Chang, Shuju Chen, Jian Cui *, Yehai Yan *

Key Lab of Rubber-plastics, Ministry of Education/Shandong Provincial Key Lab of Rubber-plastics, School of Polymer Science and Engineering, Qingdao University of Science and Technology, Qingdao 266042, China

ARTICLE INFO

Article history:
Received 5 July 2016
Received in revised form 5 September 2016
Accepted 21 September 2016
Available online 22 September 2016

Keywords:
Epoxy
Epoxide-functionalized graphene
Composite
Dispersibility
Interfacial adhesion
Properties

ABSTRACT

Uniform dispersion and strong interfacial adhesion are two critical prerequisites for application of graphene in the polymer composites. To equip the composites with multifunctional character, as little damage as possible to intrinsic structure of pristine graphene (*p*G) is also normally required. With these ends in view, an epoxide-functionalized graphene (G-EP) was designed, synthesized, and applied for developing the high-performance and multifunctional epoxy composites. Since the structure and properties of *p*G are largely inherited and the introduced epoxide moieties ensure the good dispersion and covalent connection to epoxy network, G-EP exhibits an outstanding filler efficiency compared with *p*G and other graphenic fillers previously explored in epoxy matrix. The resultant composite with only 1.0 wt% G-EP acquires 116% and 96% increments in tensile strength and Young's modulus, respectively, relative to neat epoxy. Furthermore, the electrical percolation threshold is down to 0.16 vol% (0.33 wt%) G-EP, and the thermal conductivity (TC) reaches up to 3.138 W/(m K) at 10 wt.% G-EP that corresponds to a TC increment of 189% per 1.0 wt% G-EP loading or 370% per 1.0 vol% loading. A new type of high-performance, multifunctional but much lightweight epoxy composites is thus in prospect.

1. Introduction

Epoxy is a well established thermoset polymer with a wide variety of applications ranging from electronics to aerospace. Despite the favorable mechanical, adhesive, and chemical and corrosion resistance properties, technical progress has put forward requirements of higher performance and multifunction on the epoxy materials. For example, in the electronics industry, the progress in miniaturizing and integrating the device components has created a need for epoxy materials with high heat dissipation ability when they are applied as the thermal interface materials [1]. In the aviation industry, there are practical demands on the electrostatic dissipation capacity and enhanced mechanical properties when the epoxy materials are used as the structural elements of large high-speed aerocrafts [2]. Filling epoxy with graphene seems to be a promising solution in meeting these objectives. The distinctive one-atom-thick planar structure along with low density and excellent mechanical, thermal, and electrical properties renders graphene an ideal nanofiller for developing the high-performance and multifunctional polymer composites [3,4]. What is more attractive is that graphene can be produced by exfoliation of graphite [5,6], affording cost advantage over carbon nanotube (CNT) that is another sort of important carbon nanofiller but produced by chemical synthesis.

* Corresponding authors.
E-mail addresses: jiancui@qust.edu.cn (J. Cui), yhyan@qust.edu.cn (Y. Yan).

http://dx.doi.org/10.1016/j.eurpolymj.2016.09.036
0014-3057/

It is well known that the practical performance of polymer composites depends not only on the inherent properties of fillers but, even more importantly, on their uniform dispersion in and strong interfacial interaction with polymer matrix. For the nanofiller of pristine graphene (*p*G), however, its highly cohesive van der Waals energy (5.9 kJ/mol) makes it hardly possible to be well dispersed in most of polymer matrices including epoxy matrix [7]. On the other hand, the weak interfacial adhesion between *p*G and polymer matrix, resulting mainly from the atomically smooth surface and chemical inertness of graphene, makes the load transfer from matrix to graphene inefficient. Fortunately, surface functionalization of graphene in either a covalent or noncovalent manner is found effective in improving both dispersion and integration of graphene in the matrix [8–10].

In comparison, the covalently functionalized graphene is usually more powerful than the noncovalently functionalziled one in terms of enhancing the mechanical properties of the resultant composites [3,4,8]. The most common strategy for covalent functionalization begins with graphene oxide (GO) as the starting material, which has abundant oxygen-rich functional groups with the C:O ratio up to 2:1 and proves to be an eminent platform for numerous chemical transformations [10–13]. However, owing to the excessive disruption of π-orbital structure of graphene, GO suffers from significant loss in electrical/thermal conductivity and thermal stability. Even after the tedious reduction processes, large defect population still remains (C:O ratio of 2.8–23.9:1) and intrinsic properties of *p*G are only partially restored [11]. Toxicity and expense of chemicals used in the preparation and reduction of GO are also issues of severe concern. For all that, the polymer/graphenic filler composites reported hitherto are prepared mostly from GO, reduced GO (*r*GO), or their derivatives. As a result, the physical properties of the obtained composites are far below the anticipated potentials. There still exists a large space to further improve the composite properties by taking some measures. For instance, a functionalized graphene that largely reserves the structure and properties of *p*G but can be tightly integrated into the matrix is taken as the graphenic filler.

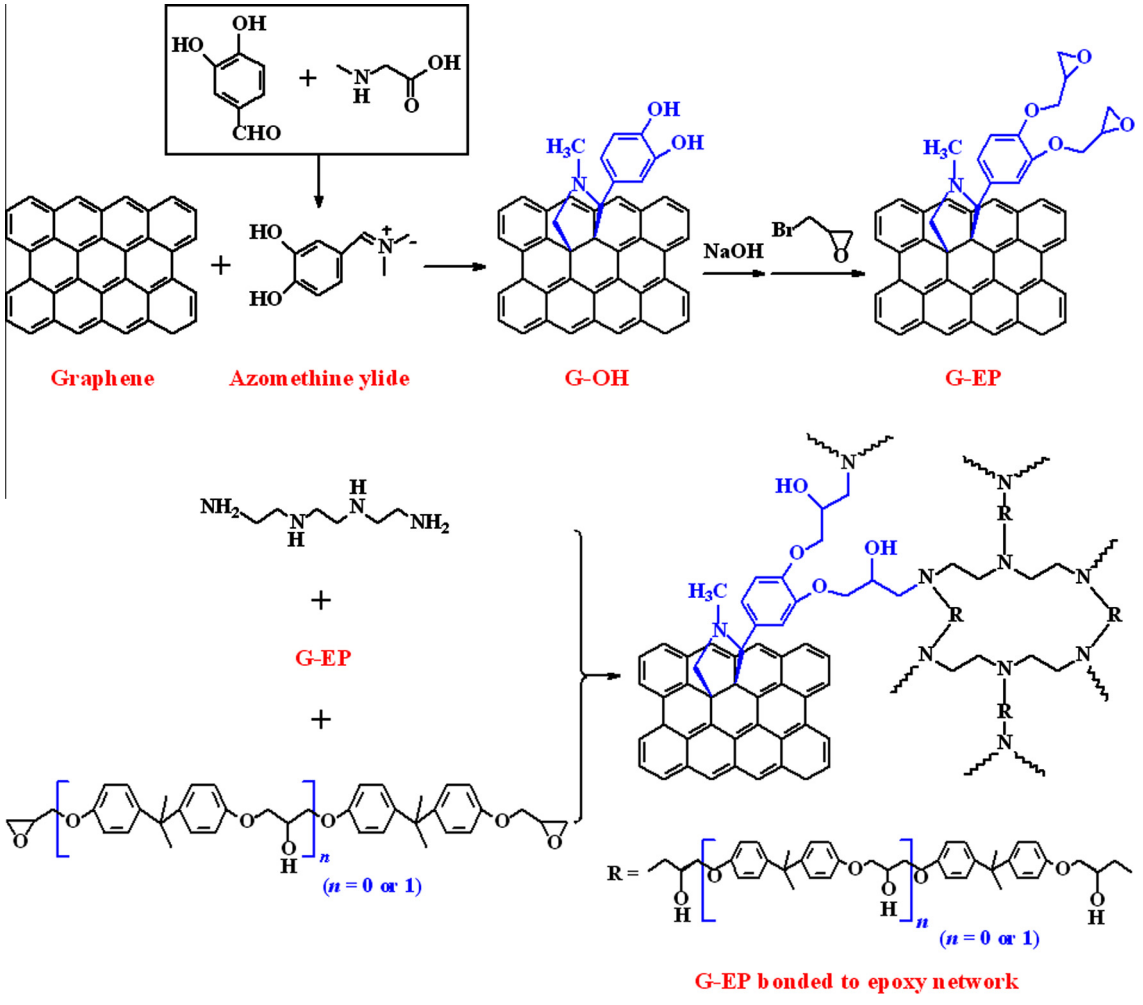

Fig. 1. Synthesis of G-EP and its application in epoxy composite.

In this respect, the covalent functionalization of *p*G by reactive moieties, such as free radical [14,15], nitrene [16], carbine [17], aryne [18], and azomethine ylide [19–24], provides a desirable option. The attached adducts with chemical reactivities allow further attachment of additional organic or inorganic components to graphene. That is, analogous to GO, these reactive moiety-functionalized graphene (RM-*f*-G) can also serve as the platform to prepare varieties of graphene-derived materials through post reactions. Meanwhile, the controllable feature of reactive moiety-based functionalization makes it highly feasible for RM-*f*-G and derivatives thereof to succeed the inherent characteristics of *p*G to a great extent, consequently supplying the desirable substitutes to GO-related fillers. With the rapid progress of top-down methods for producing graphene, such as liquid-phase exfoliation of graphite [25–27], the previous limitation for reactive moiety-based functionalization, *i.e.* availability of mass and high-quality graphene, does not exist. A recent work even showed that the graphene production rate could reach as high as 5.3 g/hr by shear exfoliation of graphite in suitable stabilizing liquid, compared with <0.6 g/hr for the GO production rate [28].

As a typical reactive moiety, azomethine ylide has been widely used for synthesis of pharmaceuticals and covalent functionalization of fullerene and carbon nanotubes through the 1,3-dipolar cycloaddition [29–31]. Recently, it was reported also applicable for functionalization of graphene [20–24]. Our work further showed that the azomethine ylide-functionalized graphene (G-OH) could serve as a versatile platform for post syntheses of various graphene-derived materials including epoxide-functionalized graphene (G-EP) (Fig. 1) [19]. In the present contribution, G-EP was systematically characterized and then employed as the functional graphenic filler for the preparation of epoxy composites through a solution-based process. Mechanical, electrical, and thermal properties of the composites were tested as a function of G-EP content. For comparison, the epoxy/*p*G composites were also prepared and investigated in parallel.

2. Experimental

2.1. Materials

Epofix from Struers was used as the epoxy matrix. It was supplied in two parts: Epofix hardener (triethylenetetramine) and Epofix resin containing 60–90% of bisphenol-A-diglycidylether ($\overline{M}_n \leq 700$) and 10–40% of alkyl (C12–C14) glycidyl ether. G-EP was synthesized starting from *p*G, which was produced by liquid-phase exfoliation of natural graphite in dimethylformamide (DMF), by a two-step reaction process, *i.e.* G-OH formation and etherification of G-OH with epibromohydrin (Fig. 1). Full details of the *p*G preparation and G-EP synthesis can be found in the Supporting Information (Parts S1–S2, Fig. S1–S5).

2.2. Preparation of epoxy composites

For preparation of the epoxy/G-EP composites, Epofix resin was mixed with the G-EP dispersion (0.62 mg/ml in DMF) in a ratio to yield the expected content of G-EP. The mixture was stirred at 500 rpm for 30 min followed by sonication (Yuhua KQ250B, 40 kHz) in a water bath for 1 hr. After complete removal of DMF, the hardener was added at a recommended weight ratio of resin/hardener = 25/3. The mixture was stirred for 3 min, cast into polytetrafluoroethylene (PTFE) mold ($60 \times 60 \times 1$ mm^3), and degassed in a vacuum oven at room temperature. Subsequently, the mixture was cured at 60 °C for 12 hr and 120 °C for 4 hr to get the final composite. By using the identical process, the epoxy/*p*G composites were also prepared.

2.3. Characterization

G-EP was characterized by using Fourier transform infrared (FTIR) spectroscopy, X-ray photoelectron spectroscopy (XPS), thermogravimetric analysis (TGA), Raman spectroscopy, atomic force microscopy (AFM), and transmission electron microscopy (TEM). FTIR spectra were recorded on a Bruker VERTEX 70 spectrometer in the transmission mode. XPS was conducted on an ESCALAB 250Xi spectrometer with a monochromatic Al Kα X-ray source ($h\nu$ = 1486 eV). All binding energies were referred to the C1s neutral carbon peak at 284.8 eV. TGA was performed with a TA-Instruments TGA Q500 apparatus at 10 °C/min heating rate in N_2 atmosphere. Raman spectra were collected on a Renishaw inVia micro-Raman spectrometer with a 532 nm Ar laser excitation. For AFM analysis, the sample was prepared by placing a drop of diluted G-EP dispersion (~5 μg/ml in chloroform) on a freshly cleaved mica substrate, residing for 30 s and sweeping off the liquid by compressed air, followed by immediate observation using a Multimode 8 AFM microscope in tapping mode. TEM was conducted on a JEOL JEM-2100 microscope with 200 kV accelerating voltage.

The dispersion state of G-EP or *p*G in epoxy matrix was studied by optical microscopy (OM), scanning electron microscopy (SEM), and TEM. OM was conducted on an Olympus BX2 microscope equipped with an Olympus DP71 camera. SEM was performed on a JEOL JSM-7500F microscope with 5 kV accelerating voltage. For TEM observations, the ultrathin sections of cast composites with ~50 nm thickness were prepared by using an ultramicrotome Leica EM UC7 equipped with a diamond knife.

For tensile tests, epoxy and its composites were cut into rectangular specimens with dimensions of $60 \times 10 \times 1$ mm^3. The tensile properties were measured using a Zwick/Roell Z030 universal testing machine at a crosshead speed of 5 mm/min. All electrical conductivity measurements were done at room temperature and 50 ± 10% relative humidity. The volume

conductivities lower than 10^{-5} S/cm were measured using a PC68 high resistance meter, whereas higher than 10^{-5} S/cm were measured by a standard four-probe method using a MODEL SZT-2000 instrument. The thermal performance was evaluated by thermal conductivity analysis and TGA. Thermal conductivities of disk-shaped epoxy and its composite samples with 50 mm diameter and 1 mm thickness were measured using a TA Instruments DTC-300 analyzer according to the ASTM E1530 guarded heat flow meter method. TGA was conducted as described for G-EP.

3. Results and discussion

The FTIR study confirmed that the epoxide moieties have been included in G-EP (Fig. 2a). Compared with G-OH, two new peaks at 813 and 1258 cm^{-1}, corresponding to the stretching of C—O—C in the epoxide ring, appear in the spectrum of G-EP. Another new peak at 1102 cm^{-1}, assigned to the stretching of C—O—C in the open-chain ether, and the noticeably increased intensity ratio of C—H stretching (2920 and 2856 cm^{-1}) to O—H stretching (3420 cm^{-1}) suggest that the introduction of epoxide moieties is realized by consuming the —OH groups through the etherification reaction (Fig. 1). Successful synthesis of G-EP was also verified by XPS. As shown in Fig. 2b, G-EP presents the enhanced O1s signal (11.20 atom%) relative to G-OH (10.25 atom%). The O1s region can be resolved into two peaks rather than a single one in G-OH (Fig. 2c). These two peaks correspond respectively to phenol oxygen (532.8 eV) and epoxide oxygen (534.2 eV) with a peak area ratio of 25:13, indicating that ~34% of —OH groups have been consumed for introducing the epoxide moieties. According to a TGA method proposed by Georgakilas et al. [20], the amount of glycidyl moieties in G-EP is determined to be ~2.4 wt% (Fig. S6).

As a result of the introduction of epoxide moieties, the Raman intensity ratio of D-band (~1330 cm^{-1}) to G-band (~1580 cm^{-1}), denoted as I_D/I_G that has been widely used as an indication of the defect content of graphene, increases from

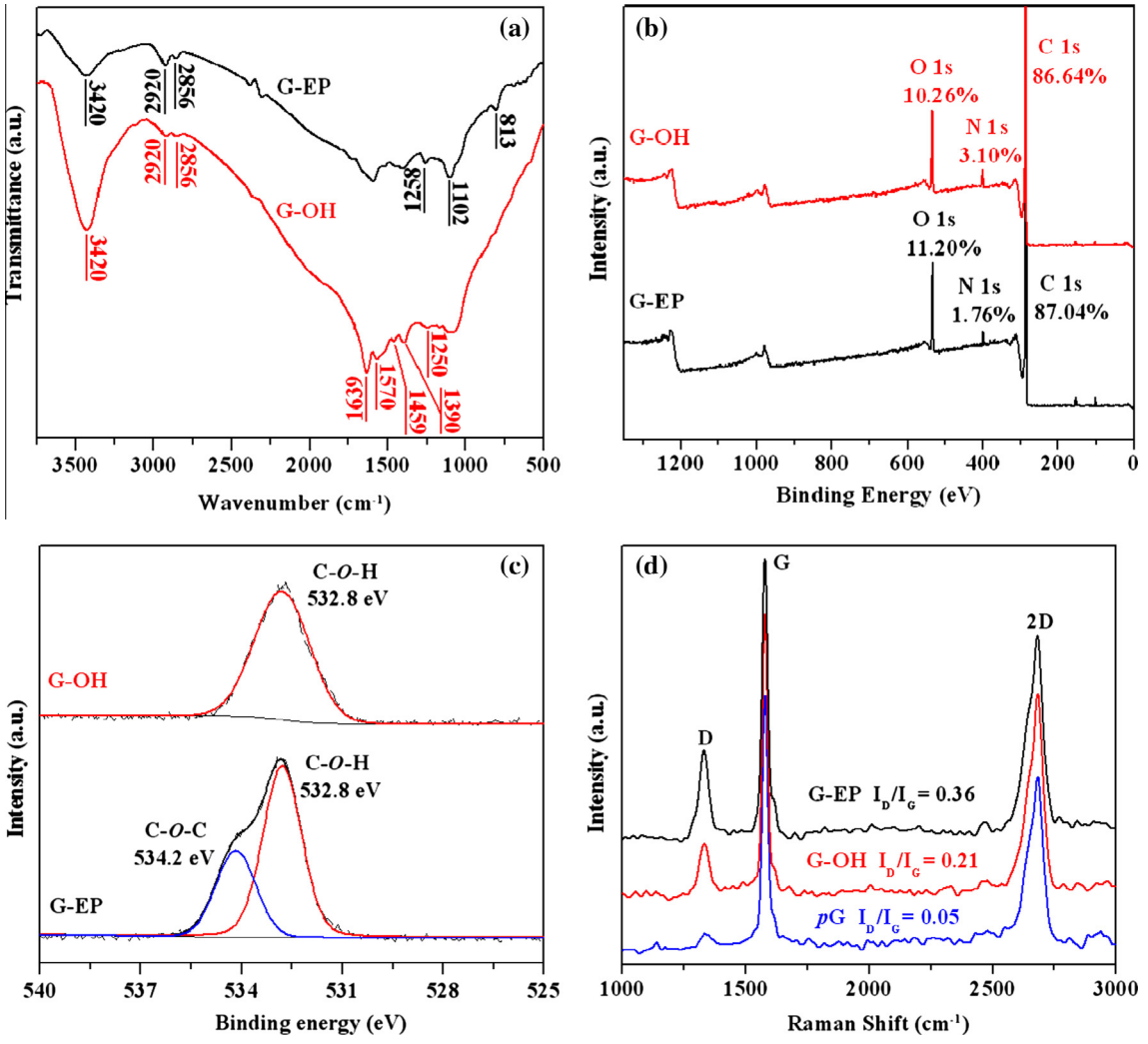

Fig. 2. (a) FTIR spectra of G-OH and G-EP, (b and c) XPS spectra of G-OH and G-EP, and (d) Raman spectra of *p*G, G-OH, and G-EP.

0.05 for *p*G and 0.21 for G-OH to 0.36 for G-EP (Fig. 2d). Even so, it is still much lower than that of *r*GO produced from reduction of GO by hydrazine (I_D/I_G = 1.44) [32] or sodium borohydride (I_D/I_G = 1.08) [33]. As a corresponding response, G-EP shows an electrical conductivity of 102 S/cm, compared with 500 S/cm for *p*G, 167 S/cm for G-OH, 0.05–500 S/cm (most common values of 10–100 S/cm) for *r*GO [34], and ~10^{-4} S/cm for GO [11]. Moreover, G-EP exhibits a good dispersing ability in DMF, tetrahydrofuran (THF), and chloroform with the maximal dispersibility of 0.62 mg/ml in DMF (Table S1), paving the way for preparation of the epoxy/G-EP composites by a solution-based process.

The dimensions of G-EP sheets were examined by AFM. Shown in Fig. 3a is a typical AFM height image with the cross-section measurements. Statistics on 102 different flakes shows that the thickness is predominantly in the range of 1.3–3.1 nm with the mean value of 2.2 nm (Fig. 3b-i). Considering that the AFM thickness of pristine monolayer graphene generally falls in 0.6–0.9 nm [35,36], the increased thickness of 1.3–3.1 nm suggests that 93% of the detected flakes are single- (10%), double- (19%), and few-layer (3- to 5-layer, 64%) graphene sheets attached with epoxide-containing adducts. The length and width of G-EP sheets were measured to be 0.2–2.9 μm (Fig. 3b-ii) and 0.16–1.9 μm (Fig. 3b-iii), respectively, with the mean values of 0.75 μm and 0.52 μm. Within the instrument resolution, no holes or other damage were detected on the basal plane, suggesting that the G-EP sheets are of good quality. This got further support from the TEM study. Fig. 3c and d presents two typical TEM images with different magnifications. All the observed G-EP sheets have smooth surface and well-resolved edges. The selected area electron diffraction (SAED) patterns exhibit the distinctive sixfold symmetry expected for graphene [37], implying that the azomethine ylide functionalization and subsequent epoxide introduction do not induce the evident lattice defects within the graphene framework. A representative SAED pattern is given in the inset of Fig. 3d.

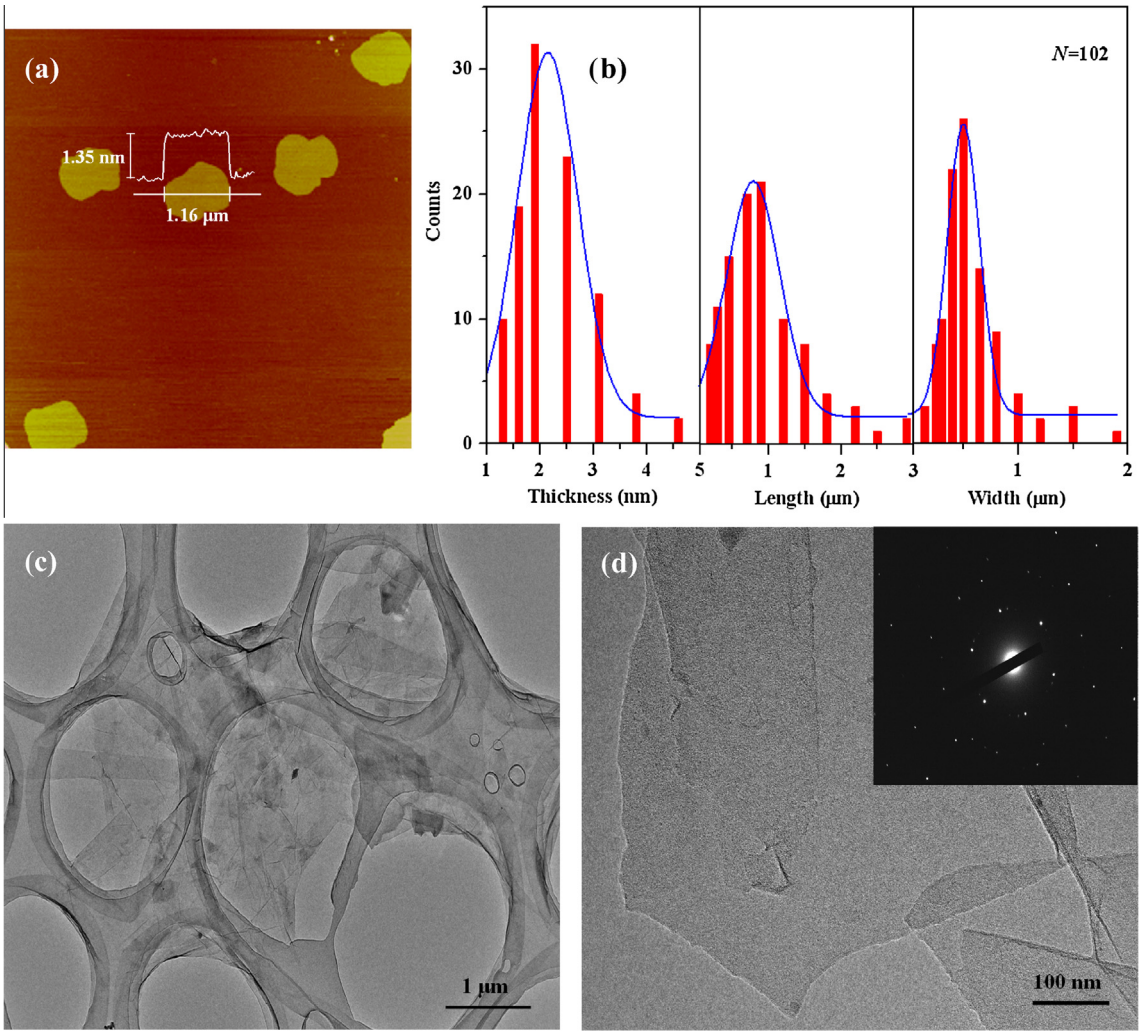

Fig. 3. (a) A typical AFM image of G-EP sheets with the cross-section measurements, (b) distributions of thickness (i), length (ii), and width (iii) of G-EP sheets, (c and d) two typical TEM images of G-EP sheets (Inset: SAED pattern of the framed area).

Table 1
Tensile properties of epoxy and its composites. Datum within parentheses is % increase relative to neat epoxy.

G-EP or *p*G content (wt%)	Tensile strength (MPa)		Young modulus (GPa)		Elongation at break (%)	
	Epoxy/*p*G	Epoxy/G-EP	Epoxy/*p*G	Epoxy/G-EP	Epoxy/*p*G	Epoxy/G-EP
0	34.0 ± 3.3		2.5 ± 0.2		1.4 ± 0.1	
0.1	35.0 ± 3.2 (3)	36.8 ± 3.6 (8)	3.0 ± 0.2 (20)	3.4 ± 0.3 (36)	1.4 ± 0.3 (0)	1.4 ± 0.2 (0)
0.3	38.4 ± 3.3 (13)	48.9 ± 3.8 (44)	3.2 ± 0.4 (28)	3.9 ± 0.5 (56)	1.2 ± 0.2 (−14)	1.4 ± 0.5 (0)
0.5	42.5 ± 4.6 (25)	61.1 ± 3.7 (80)	3.7 ± 0.5 (48)	4.3 ± 0.2 (72)	1.2 ± 0.4 (−14)	1.3 ± 0.4 (−7)
1.0	46.9 ± 4.9 (38)	73.3 ± 4.1 (116)	4.4 ± 0.6 (76)	4.9 ± 0.4 (96)	1.0 ± 0.3 (−29)	1.2 ± 0.2 (−14)
2.0	46.2 ± 4.8 (36)	53.7 ± 4.4 (58)	4.4 ± 0.6 (76)	5.2 ± 0.7 (108)	0.9 ± 0.2 (−36)	1.1 ± 0.3 (−21)
5.0	41.6 ± 4.7 (22)	50.3 ± 4.5 (48)	4.6 ± 1.1 (84)	5.6 ± 1.0 (124)	0.7 ± 0.3 (−50)	1.0 ± 0.2 (−29)

G-EP was then used for preparation of the epoxy composites. For comparison, *p*G was also employed. Table 1 summarizes the tensile properties of neat epoxy and its composites. Each datum reported here is an average of at least five measurements. In general, addition of G-EP or *p*G improves both tensile strength and Young's modulus of epoxy. At a fixed filler content, the epoxy/G-EP composite always shows superior tensile performance to the epoxy/*p*G one. The enhancement effect of graphenic filler on epoxy has also been previously reported. Depending on the functionalization of graphene and sort of epoxy (rubbery or glassy one), the resultant composites usually showed the increments in strength ranging from 0.9–269% and in modulus from 6% to 536% over neat epoxy (Table S2). In this work, the epoxy/G-EP composite was prepared from the epoxide-functionalized graphene and glassy epoxy. Its strength increases with the increase of G-EP and reaches 73.3 MPa at 1.0 wt% G-EP, representing a 116% increment relative to neat epoxy (34.0 MPa). Thereafter, further increasing the G-EP content leads to the weakening of strength. In contrast, the modulus increases continuously with increase of G-EP. The 96% and 124% gains over neat epoxy (2.5 GPa) are achieved at 1.0 wt% and 5.0 wt% G-EP, respectively. To our knowledge, these increment values are among the highest ones ever reported thus far for composites prepared from the glassy epoxy (Table S2: ⩽97% in strength and ⩽114% in modulus), although the increment in strength (116%) is still inferior to that of composite prepared from the glassy epoxy but with aligned *r*GO (500% increment) [38] or three-dimensional *r*GO skeleton (141% increment) [39]. Furthermore, addition of G-EP only slightly reduces the elongation at break (Table 1), indicating that the toughness of epoxy is not evidently weakened.

The Halpin-Tsai model, which was well established for fiber-reinforced composites and had been recently extended to CNT- and graphenic filler-filled composites [40–44], was employed here to theoretically predict the Young's modulus of epoxy/G-EP composite. For this, it was assumed that the G-EP sheets work as rectangular solid fibers and are dispersed separately and uniformly in the epoxy matrix. The Young's moduli of composites with randomly dispersed (E_r) and aligned (E_a) G-EP (parallel to the composite film surface) are defined as the following modified Halpin-Tsai equations [40–43]:

$$E_r = E_{EP}\left(\frac{3}{8}\frac{1+\eta_L\xi V_f}{1-\eta_L V_f}+\frac{5}{8}\frac{1+2\eta_W V_f}{1-\eta_W V_f}\right) \tag{1}$$

$$E_a = E_{EP}\left(\frac{1+\eta_L\xi V_f}{1-\eta_L V_f}\right) \tag{2}$$

where

$$\eta_L = \frac{E_f/E_{EP}-1}{E_f/E_{EP}+\xi} \tag{3}$$

$$\eta_W = \frac{E_f/E_{EP}-1}{E_f/E_{EP}+2} \tag{4}$$

$$\xi = \frac{\overline{W}+\overline{L}}{\overline{t}} \tag{5}$$

E_f and E_{EP} are the Young's moduli of G-EP (assumed as the graphene modulus of 1.0 TPa [34]) and epoxy matrix. V_f is the volume fraction of G-EP in the composite and estimated based on the assumed G-EP density of 2.28 g/cm^3 and epoxy density of 1.10 g/cm^3. $\overline{L}$, $\overline{W}$, and $\overline{t}$ refer to the mean length, width, and thickness of the G-EP sheets, respectively.

Fig. 4 shows the predicted Young's modulus according to Eqs. (1)–(5), along with the experimental one, as a function of volume fraction of G-EP. It is interesting to find that when the G-EP content is no higher than 0.48 vol% (1.0 wt%) the experimental result agrees well with the theoretical prediction for composite with G-EP presumably aligned parallel to the film surface. Beyond this critical G-EP content, the experimental modulus becomes more approximate to the predicted one under the assumption that G-EP is randomly dispersed in epoxy matrix. Such phenomenon is believed to occur due to the large planar structure of G-EP sheets and low viscosity of solution-based processing system [38]. Triggered by a thermodynamic drive to minimize the system free energy, G-EP sheets are randomly dispersed in the primary solution.

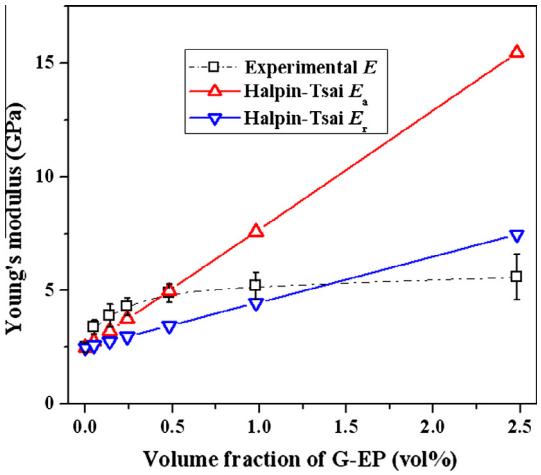

Fig. 4. Young's modulus as a function of volume fraction of G-EP.

Upon gradual removal of DMF, the excluded volume effect [45,46], which prevails at a low G-EP content, actuates G-EP sheets to align in parallel. At a high content, however, the steric hindrance imposed by the dense G-EP sheets causes a significant energy barrier that restrains the free movement of G-EP sheets to find their most favorable configuration, *i.e.* alignment to each other [46].

For exploring the reinforcement mechanism, the OM study was conducted on the uncured epoxy/G-EP (1.0 wt%) mixture, and the SEM study was performed on the corresponding cured composite. As shown in Fig. 5a, the uncured mixture (thickness ~15 μm) coated on a glass slide looks nearly clear and uniform under the optical microscope. Correspondingly, the SEM image of the fracture surface of cured composite exhibits that the G-EP sheets are uniformly dispersed in the epoxy matrix (Fig. 5b). Closer inspection (inset of Fig. 5b) shows that the dispersed sheets contact tightly with the surrounding epoxy, suggesting formation of the excellent epoxy/G-EP interfacial adhesion. On the contrary, many dark spots with several micrometer diameters are observed on the optical image of the uncured epoxy/*p*G mixture (Fig. 5c). The SEM study reveals that the spots are actually the *p*G agglomerates, presenting a very poor dispersing state (Fig. 5d). Owing to the weak interfacial interaction, it is easy to observe many slender cavities left by the pull-out of *p*G sheets and big gaps between *p*G sheets and matrix (inset of Fig. 5d). What is generally accepted is that the good dispersion of particles, especially nanoparticles, in the matrix is beneficial for reducing stress concentration centers, affording more uniform stress distribution, and enlarging interfacial area for efficient load transfer [47]. Formation of strong interfacial interaction between matrix and particles strengthens these effects. From the OM and SEM studies, it is clear that the epoxide functionalization realizes both uniform dispersion of G-EP sheets and their strong interaction with the epoxy matrix, thus giving rise to the superior tensile performance of resultant composites. The necessity of previous epoxide functionalization of graphene sheets was argued by a control experiment in which the azomethine ylide, in-situ formed by condensation of sarcosine and 3,4-dihydroxybenzaldehyde [19], and epibromohydrin were directly added into the mixture of epoxy and *p*G (1.0 wt%) for preparation of the composite. Both OM and SEM observations indicate that the dispersion quality of graphene sheets in epoxy matrix is much poorer than G-EP but very resembles *p*G (Fig. S7). Despite having good dispersion ability, it is a pity that there still exists an upper limit for G-EP to be well dispersed in the epoxy matrix. As displayed in Fig. 5e and f, the G-EP sheets tend to aggregate in some sense when the content increases to 2.0 wt%. Such observation makes a good correlation with the tensile testing results.

The local charging of epoxy around the G-EP or *p*G sheets makes it difficult for SEM to resolve the dimensions, especially thickness, of the dispersed sheets. In view of the penetrability of electron beam and the ability to identify monolayer graphene with angstrom resolution, TEM was applied to fulfill this task by taking the composite loaded with 1.0 wt% G-EP or *p*G as the typical sample. Under a low magnification, many dark spots are observed on the *p*G-containing sample (Fig. S8a). The magnified image reveals that the spots are actually agglomerates of *p*G sheets with a lateral size of 1–3 μm (Fig. 6a). In contrast, the epoxy/G-EP composite sample appears clear, transparent, and consistent under the same low magnification, hinting no aggregation and/or restacking of G-EP sheets (Fig. S8b). Closer observation corroborates that the G-EP sheets are separately dispersed in the epoxy matrix (Fig. 6b). Despite being clothed by the matrix, the edges of G-EP sheets can be reasonably resolved, thus allowing one to roughly determine their lateral sizes. On the statistics of 38 objectives, the mean value is estimated to be 0.7 ± 0.5 μm, which is basically in accordance with that of G-EP before being filled, suggesting that the composite processing conditions adopted here have little effect on the lateral size of G-EP. By comparing the intensity ratios of {1 1 0 0} spots to {2 1 1 0} ones of the SAED patterns, most of the dispersed G-EP sheets were identified to be of monolayer and few-layer characters [48]. The inset of Fig. 6b shows a SAED pattern of a typical monolayer G-EP sheet, where the {1100} spots are significantly more intensive than the {2 1 1 0} ones.

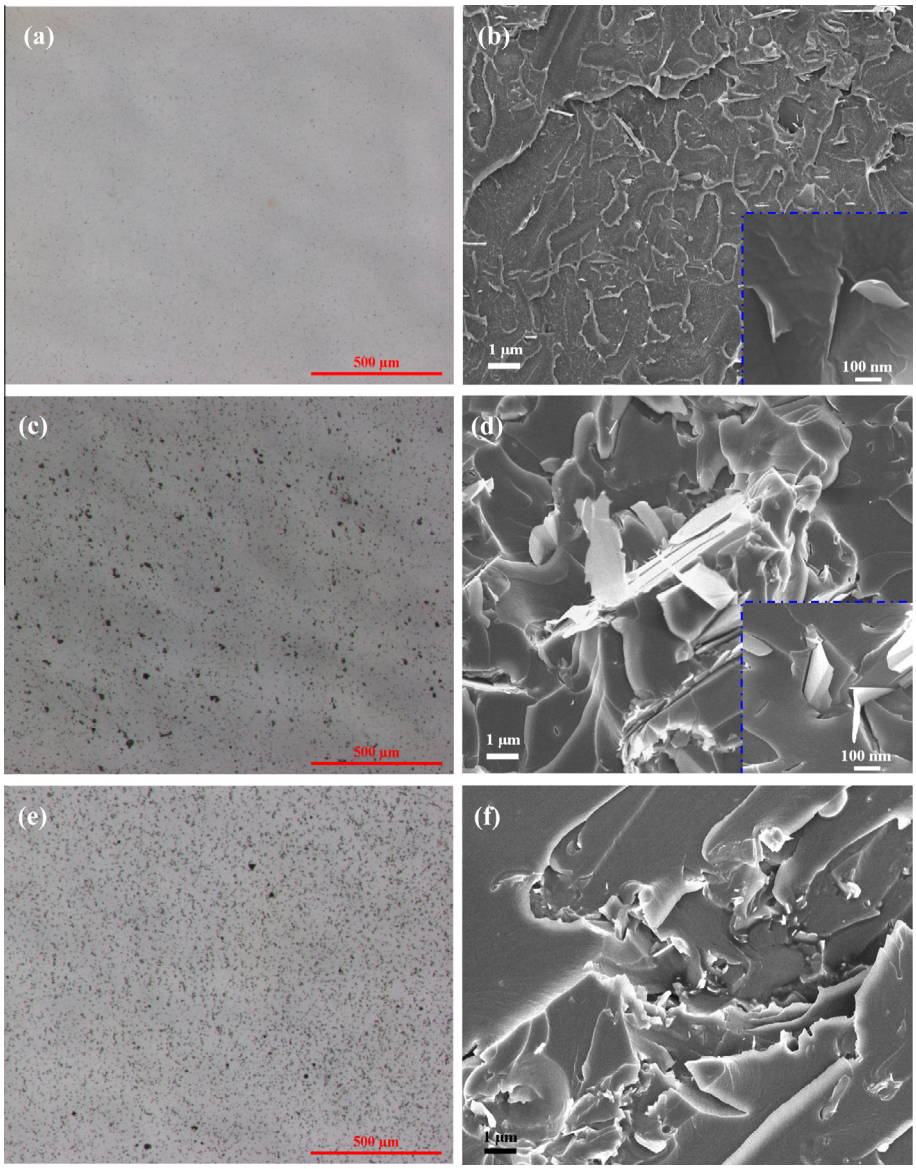

Fig. 5. Optical images of (a) 1.0 wt% G-EP, (c) 1.0 wt% *p*G, and (e) 2.0 wt% G-EP dispersed in epoxy matrix before curing (scale bar – 500 μm); SEM images of epoxy composites with (b) 1.0 wt% G-EP, (d) 1.0 wt% *p*G, and (f) 2.0 wt% G-EP (scale bar – 1 μm).

The enhanced interfacial interaction is attributed to the covalent bonding of G-EP sheets with epoxy matrix (Fig. 1). To verify the formation of new bonds, a model study was carried out. For this, G-EP was mixed with 10 wt% Epofix hardener and then thermally treated at the curing condition of composites. After that, the excess hardener was thoroughly removed by dialyzing with 3500 Da MWCO dialysis membrane of regenerated cellulose (Fisher) for 24 hr. The FTIR spectra show that the peaks for epoxide moieties (813 and 1258 cm^{-1}) from G-EP (Fig. 7a) disappear in the thermally treated sample (Fig. 7c). Instead, a new peak corresponding to O-H bending appears at 1312 cm^{-1}. The strong and broad peak in the range of 3000–3700 cm^{-1} is assigned to the overlap of O—H stretching and N—H stretching of the —NH_2 (3353 cm^{-1}) and —NH— (3278 cm^{-1}) moieties from Epofix hardener (Fig. 7b). These spectral changes clearly manifest the reaction of G-EP with Epofix hardener.

Next, the electrical conductivities of epoxy/G-EP composites were evaluated. As shown in Fig. 8a, increasing G-EP content (ϕ) remarkably improves the conductivity (σ), particularly at the low G-EP content, showing a typical percolation behavior. At 0.48 vol% (1.0 wt%) G-EP, the σ value reaches 7.8×10^{-8} S/cm, already meeting the criterion for antistatic material (10^{-8} S/cm) [49]. An impressive contrast is that at least 0.98 vol% (2.0 wt%) *p*G (the corresponding composite shows $\sigma = 9.2 \times 10^{-9}$ S/cm, Fig. S9) or 8–20 wt% carbon black should be added for achievement of such an antistatic material

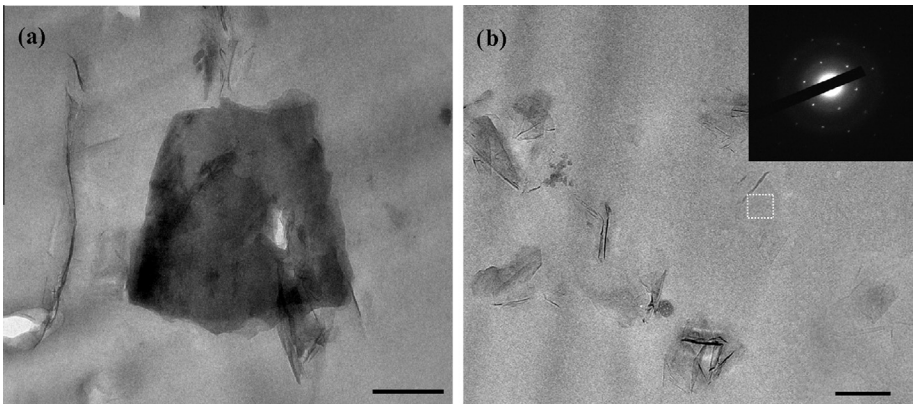

Fig. 6. TEM images of epoxy composites with (a) 1.0 wt% *p*G and (b) 1.0 wt% G-EP (Scale bar: 500 nm; Inset: SAED pattern of the framed area).

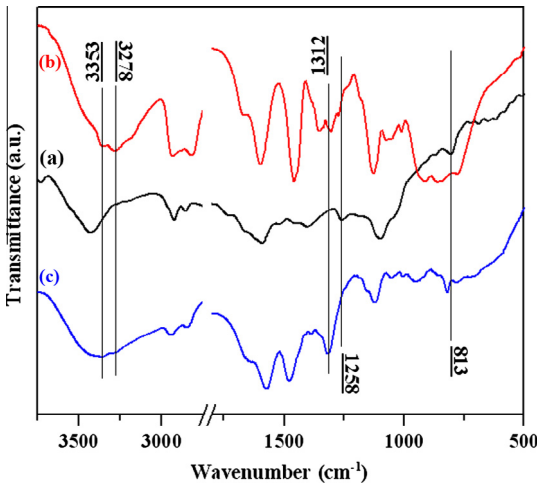

Fig. 7. FTIR spectra of (a) G-EP, (b) Epofix hardener, and (c) thermally treated G-EP/Epofix hardener sample with 10 wt% Epofix hardener.

[50]. Therefore, it is very promising for G-EP to be applied as an effective conductive filler for developing the antistatic but much lightweight epoxy materials. The dependency of σ on ϕ can be described using the power law [2]:

$$\sigma = \sigma_f[(\phi - \phi_c)/(1 - \phi_c)]^t, \text{ for } \phi > \phi_c \quad (6)$$

where σ_f is the conductivity of filler, ϕ_c is the percolation volume fraction, and t is the critical exponent.

By evaluating the linearity of the $\log\sigma$ *vs* $\log[(\phi - \phi_c)/(1 - \phi_c)]$ graph (Fig. 8b), ϕ_c is determined to be 0.16 vol% (0.33 wt %), suggesting that only 0.16 vol% G-EP is sufficient to construct an effective conductive path in epoxy matrix. This threshold value is among the lowest ones reported for epoxy composites with graphenic fillers (Table S3: 0.05–1.0 vol%) and very close to the theoretically computed one with the overlapping oblate ellipsoids/disks (~0.1 vol%) [51]. It results mainly from the low defect content of G-EP (Fig. 2d) and its good dispersion in epoxy matrix (Fig. 5 and 6). Also, the linear fit gives $\sigma_f = 10^{5.89}$ S/cm that approaches the theoretical limit of monolayer graphene (10^6 S/cm) [52], compared with $10^{6.39-6.55}$ and $10^{4.92}$ S/cm for *r*GO in polycarbonate [2] and polystyrene composites [49], respectively. The critical exponent, t, is determined to be 4.33, which is higher than the values of ~2.0 usually reported for CNT filled polymer composites [53–56] but falls in the range of 2.40–6.92 often found in graphenic filler-containing polymer composites including epoxy ones (Table S3). The high t value may be due to the extreme geometries of graphenic fillers, indicating a different electron transport behavior [2,57].

The thermal performance of epoxy/G-EP composite was characterized in terms of thermal conductivity (TC) and thermal stability. Fig. 9a depicts the dependence of TC on the G-EP content. It is noted that TC increases monotonously from 0.158 W/(m K) for neat epoxy to 3.138 W/(m K) for composite with 10 wt% G-EP, representing an increment of 1886%. Similar ever-increasing behavior takes also place on the epoxy/*p*G composite (Fig. 9b). In stark contrast, however, the latter only acquires TC of 0.652 W/(m K) at 10 wt% *p*G (311% increment over neat epoxy). In reference to a polymer system loaded with thermal conductive filler, the heat transport/dissipation proceeds principally in the form of phonons or lattice vibration,

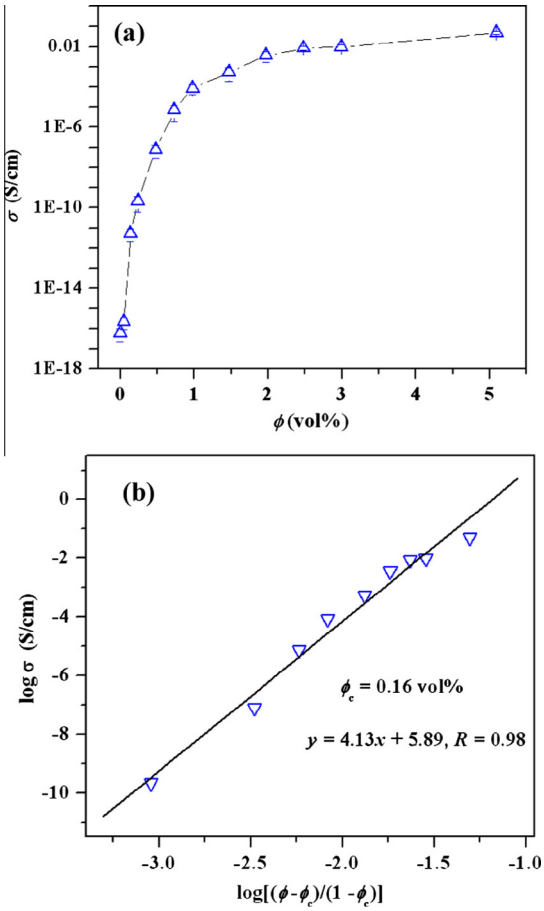

Fig. 8. (a) Electrical conductivity (σ)of epoxy/G-EP composite as a function of G-EP content (ϕ), (b) linear behavior of logσ against log$[(\phi - \phi_c)/(1 - \phi_c)]$.

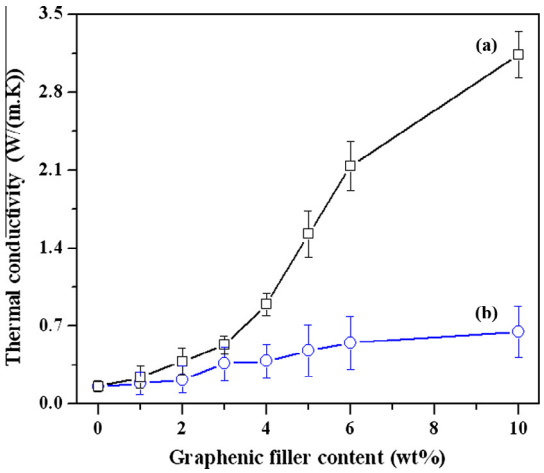

Fig. 9. TC of epoxy composites as a function of (a) G-EP and (b) *p*G contents.

and the poor phonon coupling in the vibration modes at the filler-polymer and filler-filler interfaces usually causes serious thermal resistance [3]. Therefore, in addition to the factor of filler intrinsic TC, the thermal conductive performance of polymer composites is also governed by filler dispersion quality and nature of filler-polymer interface. Thanks to the inclusion of glycidyl moieties, G-EP realizes the high-quality dispersion and enhanced interfacial bonding with epoxy matrix (Figs. 5–7), facilitating the phonon transfer from G-EP to epoxy matrix and minimizing the phonon scattering and interfacial thermal

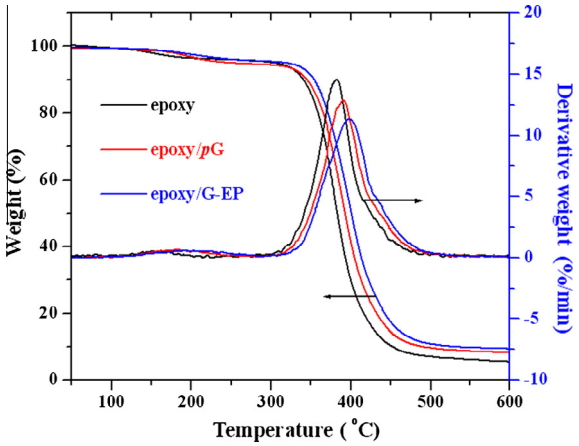

Fig. 10. Typical TGA curves of epoxy and its composites.

Table 2
T_o and T_p of epoxy and its composites.

G-EP/*p*G content (wt%)		0	0.5	1.0	2.0
T_o (°C)	Epoxy/*p*G	319	318	321	320
	Epoxy/G-EP		324	333	334
T_p (°C)	Epoxy/*p*G	382	384	389	390
	Epoxy/G-EP		382	398	392

resistance. Moreover, the low defect content (Fig. 2d) and thus high TC close to that of *p*G ensures G-EP to be capable of functioning as the highly conductive channel for heat transport. It is hence not surprising for G-EP rather than *p*G to be more competent for developing the thermal conductive epoxy composites. Actually, even compared with other graphenic fillers that have been previously explored in epoxy matrix, G-EP also behaves very outstanding. Its filler efficiency, defined as the TC increment % per 1.0 wt% loading (TCI_w) or per 1.0 vol% loading (TCI_v), reaches TCI_w = 189 or TCI_v = 370. This is much superior or comparable to that of most other graphenic fillers (Table S3, TCI_w = 5–175) and only inferior to that of assembled aligned graphene platelets (TCI_w = 1412) [58], noncovalently functionalized *r*GO (TCI_W = 213 and 600) [59,60], and core-shell structured polymethyl methacrylate-*r*GO additive (TCI_w = 700) [61]. These results firmly endorse that G-EP is an extremely efficient filler in enhancing TC, especially considering that the traditional fillers usually present a TCI_v of ~20 [57].

The thermal stability was examined by TGA. As typically presented in Fig. 10, all samples show a similar thermolysis behavior with the thermograms characterizing one thermolytic zone. Both onset decomposition temperature (T_o) and peak decomposition temperature (T_p) extracted from the thermograms indicate that addition of G-EP or *p*G improves the thermal stability of epoxy (Table 2). The improved thermostability could be due to the enhanced barrier property endowed by G-EP or *p*G that prevents the outside oxygen from penetrating into the composite to induce the oxidation of epoxy and the excellent thermal conductor role played by G-EP or *p*G that dissipates heat from the surroundings and avoids formation of the hot spots [3]. Moreover, G-EP or *p*G may also act as an efficient radical catcher to prevent epoxy from decomposition [8]. For these effects, it is assuredly critical for G-EP or *p*G to be well dispersed and form an effective thermal conductive path in the matrix. This explains why the composite loaded with 1.0 wt% G-EP has the optimal thermal stability with the respective T_o and T_p lags of 14 and 16 °C. At this loading, G-EP is still dispersed well in matrix and the thermal conductive path may have been formed. Beyond this loading, *e.g.* at 2.0 wt%, G-EP tends to aggregate (Figs. 5 and 6 and S2).

4. Conclusions

By applying G-EP as a functional filler, the high-performance, multifunctional but lightweight epoxy composites were developed. In particular, G-EP was shown to perform significantly better than *p*G and overwhelming majority of previously explored graphenic fillers in enhancing a variety of physical properties of epoxy including tensile strength, Young's modulus, electrical conductivity, TC, and thermal stability. Three main factors contribute to these great enhancements. First, the controllable functionalization ensures the excellent properties of *p*G largely inherited by G-EP. Second, the introduced epoxide moieties facilitate G-EP to be well dispersed in epoxy matrix. Third, the covalent reaction between G-EP and Epofix hardener strengthens the mechanical adhesion at the filler-matrix interface. The demonstrated philosophy of interface molecular engineering of graphene/epoxy composite system that proceeds through the appropriate functionalization of graphene may be extended to other graphene/polymer systems, providing a general strategy for developing the desirable graphene/polymer composites.

Acknowledgments

This work was supported by the NSF of China (No. 51303090 and 51373087), NSF of Shandong Province (No. ZR2014EMP008), and Taishan Mountain Scholar Constructive Engineering Foundation.

Appendix A. Supplementary material

Supplementary data associated with this article can be found, in the online version, at http://dx.doi.org/10.1016/j.eurpolymj.2016.09.036.

References

[1] R.S. Prasher, J.-Y. Chang, I. Sauciuc, S. Narasimhan, D. Chau, G. Chrysler, et al, Nano and micro technology-based next-generation package-level cooling solutions, Int. Technol. J. 9 (2005) 285–296.
[2] M. Yoonessi, J.R. Gaier, Highly conductive multifunctional graphene polycarbonate nanocomposites, ACS Nano 4 (2010) 7211–7220.
[3] H. Kim, A.A. Abdala, C.W. Macosko, Graphene/polymer nanocomposites, Macromolecules 43 (2010) 6515–6530.
[4] X. Huang, X. Qi, F. Boey, H. Zhang, Graphene-based composites, Chem. Soc. Rev. 41 (2012) 666–686.
[5] M. Yi, Z. Shen, A review on mechanical exfoliation for the scalable production of graphene, J. Mater. Chem. A 3 (2015) 11700–11715.
[6] M. Cai, D. Thorpe, D.H. Adamson, H.C. Schniepp, Methods of graphite exfoliation, J. Mater. Chem. 22 (2012) 24992–25002.
[7] R. Zacharia, H. Ulbricht, T. Hertel, Interlayer cohesive energy of graphite from thermal desorption of polyaromatic hydrocarbons, Phys. Rev. B 69 (2004) 155406.
[8] V. Georgakilas, M. Otyepka, A.B. Bourlinos, V. Chandra, N. Kim, K. Christian Kemp, et al, Functionalization of graphene: covalent and non-covalent approaches, derivatives and applications, Chem. Rev. 112 (2012) 6156–6214.
[9] L. Rodriguez-Perez, M.A. Herranza, N. Martin, The chemistry of pristine graphene, Chem. Commun. 49 (2013) 3721–3735.
[10] S. Eigler, A. Hirsch, Chemistry with graphene and graphene oxide - challenges for synthetic chemists, Angew. Chem. Int. Ed. 53 (2014) 7720–7738.
[11] D.R. Dreyer, S. Park, C.W. Bielawski, R.S. Ruoff, The chemistry of graphene oxide, Chem. Soc. Rev. 39 (2010) 228–240.
[12] D. Chen, H. Feng, J. Li, Graphene oxide: preparation, functionalization, and electrochemical applications, Chem. Rev. 112 (2012) 6027–6053.
[13] D.R. Dreyer, A.D. Todd, C.W. Bielawski, Harnessing the chemistry of graphene oxide, Chem. Soc. Rev. 43 (2014) 5288–5301.
[14] E. Bekyarova, M.E. Itkis, P. Ramesh, C. Berger, M. Sprinkle, W.A. de Heer, et al, Chemical modification of epitaxial graphene: spontaneous grafting of aryl groups, J. Am. Chem. Soc. 131 (2009) 1336–1337.
[15] K.E. Whitener Jr., W.-K. Lee, N.D. Bassim, R.M. Stroud, J.T. Robinson, P.E. Sheehan, Transfer of chemically modified graphene with retention of functionality for surface engineering, Nano Lett. 16 (2016) 1455–1461.
[16] S. Xie, S.A. Lopez, O. Ramström, M. Yan, K.N. Houk, 1,3-Dipolar cycloaddition reactivities of perfluorinated aryl azides with enamines and strained dipolarophiles, J. Am. Chem. Soc. 137 (2015) 2958–2966.
[17] C.K. Chua, A. Ambrosi, M. Pumera, Introducing dichlorocarbene in graphene, Chem. Commun. 48 (2012) 5376–5378.
[18] X. Zhong, J. Jin, S. Li, Z. Niu, W. Hu, R. Li, et al, Aryne cycloaddition: highly efficient chemical modification of graphene, Chem. Commun. 46 (2010) 7340–7342.
[19] S. Zhao, H. Wang, L. Xin, J. Cui, Y. Yan, A versatile platform of 2-(3,4-dihydroxyphenyl) pyrrolidine grafted graphene for preparation of various graphene-derived materials, Chem. Asian. J. 10 (2015) 1177–1183.
[20] V. Georgakilas, A. Kouloumpis, D. Gournis, A.B. Bourlinos, C. Trapalis, R. Zboril, Tuning the dispersibility of carbon nanostructures from organophilic to hydrophilic: towards the preparation of new multipurpose carbon-based hybrids, Chem. Eur. J. 19 (2013) 12884–12891.
[21] X. Zhang, L. Hou, A. Cnossen, A.C. Coleman, O. Ivashenko, P. Rudolf, et al, One-pot functionalization of graphene with porphyrin through cycloaddition reactions, Chem. Eur. J. 17 (2011) 8957–8964.
[22] Y. Cao, K.N. Houk, Computational assessment of 1,3-dipolar cycloadditions to graphene, J. Mater. Chem. 21 (2011) 1503–1508.
[23] M. Quintana, K. Spyrou, M. Grzelczak, W.R. Browne, P. Rudolf, M. Prato, Functionalization of graphene via 1,3-dipolar cycloaddition, ACS Nano 4 (2010) 3527–3533.
[24] V. Georgakilas, A.B. Bourlinos, R. Zboril, T.A. Steriotis, P. Dallas, A.K. Stubos, et al, Organic functionalisation of graphenes, Chem. Commun. 46 (2010) 1766–1768.
[25] J.N. Coleman, Liquid exfoliation of defect-free graphene, Acc. Chem. Res. 46 (2013) 14–22.
[26] A. Ciesielski, P. Samorì, Graphene via sonication assisted liquid-phase exfoliation, Chem. Soc. Rev. 43 (2014) 381–398.
[27] V. Nicolosi, M. Chhowalla, M.G. Kanatzidis, M.S. Strano, J.N. Coleman, Liquid exfoliation of layered materials, Science 340 (2013) 1226419.
[28] K.R. Paton, E. Varrla, C. Backes, R.J. Smith, U. Khan, A. O'Neill, et al, Scalable production of large quantities of defect-free few-layer graphene by shear exfoliation in liquids, Nat. Mater. 13 (2014) 624–630.
[29] L.M. Harwood, R.J. Vickers, Azomethine ylides, in: A. Padwa, W.H. Pearson (Eds.), Synthetic Applications of 1,3-Dipolar Cycloaddition Chemistry toward Heterocycles and Natural Products, Wiley, New York, 2002, pp. 169–252.
[30] S. Aroua, Y. Yamakoshi, Prato reaction of M3N@I(h)-C80 (M = Sc, Lu, Y, Gd) with reversible isomerization, J. Am. Chem. Soc. 134 (2012) 20242–20245.
[31] V. Georgakilas, A. Bourlinos, D. Gournis, T. Tsoufis, C. Trapalis, A. Mateo-Alonso, et al, Multipurpose organically modified carbon nanotubes: from functionalization to nanotube composites, J. Am. Chem. Soc. 130 (2008) 8733–8740.
[32] V.C. Tung, M.J. Allen, Y. Yang, R.B. Kaner, High-throughput solution processing of large-scale graphene, Nat. Nanotechnol. 4 (2009) 25–29.
[33] N. Mohanty, A. Nagaraja, J. Armesto, V. Berry, High-throughput, ultrafast synthesis of solution-dispersed graphene via a facile hydride chemistry, Small 6 (2010) 226–231.
[34] V. Singh, D. Joung, L. Zhai, S. Das, S.I. Khondaker, S. Seal, Graphene based materials: past, present and future, Prog. Mater. Sci. 56 (2011) 1178–1271.
[35] S. Park, R.S. Ruoff, Chemical methods for the production of graphenes, Nat. Nanotechnol. 4 (2009) 217–224.
[36] P. Nemes-Incze, Z. Osvath, K. Kamaras, L.P. Biro, Anomalies in thickness measurements of graphene and few layer graphite crystals by tapping mode atomic force microscopy, Carbon 46 (2008) 1435–1442.
[37] J.C. Meyer, A.K. Geim, M.I. Katsnelson, K.S. Novoselov, T.J. Booth, S. Roth, The structure of suspended graphene sheets, Nature 446 (2007) 60–63.
[38] N. Yousefi, X. Lin, Q. Zheng, X. Shen, J.R. Pothnis, J. Jia, et al, Simultaneous in situ reduction, self-alignment and covalent bonding in graphene oxide/epoxy composites, Carbon 59 (2013) 406–417.
[39] Y. Ni, L. Chen, K. Teng, J. Shi, X. Qian, Z. Xu, et al, Superior mechanical properties of epoxy composites reinforced by 3D interconnected graphene skeleton, ACS Appl. Mater. Interfaces 7 (2015) 11583–11591.
[40] W.E. Mahmoud, Morphology and physical properties of poly(ethylene oxide) loaded graphene nanocomposites prepared by two different techniques, Eur. Polym. J. 47 (2011) 1534–1540.
[41] M.A. Rafiee, J. Rafiee, Z. Wang, H. Song, Z.Z. Yu, N. Koratkar, Enhanced mechanical properties of nanocomposites at low ggraphene content, ACS Nano 3 (2009) 3884–3890.
[42] P.K. Mallick, Fiber-Reinforced Composites, Dekker, New York, 1993.
[43] J.C. Halpin, R. Thomas, Ribbon reinforcement of composites, J. Compos. Mater. 2 (1968) 488–497.

[44] M.K. Yeh, N.H. Tai, J.H. Liu, Mechanical behavior of phenolic-based composites reinforced with multi-walled carbon nanotubes, Carbon 44 (2006) 1–9.
[45] J.H. Park, N.R. Aluru, Self-assembly of graphenes, Surf. Sci. 605 (2011) 1616–1620.
[46] D. Konatham, A. Striolo, Molecular design of stable graphene nanosheets dispersions, Nano Lett. 8 (2008) 4630–4641.
[47] J.N. Coleman, U. Khan, Y.K. Gun'ko, Mechanical reinforcement of polymers using carbon nanotubes, Adv. Mater. 18 (2006) 689–706.
[48] S. Horiuchi, T. Gotou, M. Fujiwara, R. Sotoaka, M. Hirata, K. Kimoto, et al, Carbon nanofilm with a new structure and property, Jpn. J. Appl. Phys. 42 (2003) L1073–L1076.
[49] S. Stankovich, D.A. Dikin, G.H.B. Dommett, K.M. Kohlhass, E.J. Zimney, E.A. Stach, et al, Graphene-based composite materials, Nature 442 (2006) 282–286.
[50] B. Potshke, T.D. Fornes, D.R. Paul, Rheological behavior of multiwalled carbon nanotube/polycarbonate composites, Polymer 43 (2002) 3247–3255.
[51] E.J. Garboczi, K.A. Snyder, J.F. Douglas, M.F. Thorpe, Geometrical percolation threshold of overlapping ellipsoids, Phys. Rev. E 52 (1995) 819–828.
[52] The ScienceDaily Online, <https://www.sciencedaily.com/releases/2008/03/080324094514.htm>, (accessed May 2016).
[53] S. Barrau, P. Demont, A. Peigney, C. Laurent, C. Lacabanne, DC and AC conductivity of carbon nanotubes-polyepoxy composites, Macromolecules 36 (2003) 5187–5194.
[54] M.N. Tchoul, W.T. Ford, M.L.P. Ha, I. Chavez-Sumarriva, B.P. Grady, G. Lolli, et al, Composites of single-walled carbon nanotubes and polystyrene: preparation and electrical conductivity, Chem. Mater. 20 (2008) 3120–3126.
[55] Y. Yan, J. Cui, S. Zhao, J. Zhang, J. Liu, J. Cheng, Interface molecular engineering of single-walled carbon nanotube/epoxy composites, J. Mater. Chem. 22 (2012) 1928–1936.
[56] Y. Yan, J. Cui, P. Potschke, B. Voit, Dispersion of pristine single-walled carbon nanotubes using pyrene-capped polystyrene and its application for preparation of polystyrene matrix composites, Carbon 48 (2010) 2603–2612.
[57] D. Stauffer, A. Aharony, Introduction to Percolation Theory, Taylor & Francis, London, 1994.
[58] Q. Li, Y. Guo, W. Li, S. Qiu, C. Zhu, X. Wei, et al, Ultrahigh thermal conductivity of assembled aligned multilayer graphene/epoxy composite, Chem. Mater. 26 (2014) 4459–4465.
[59] C.C. Teng, C.C.M. Ma, C.H. Lu, S.Y. Yang, S.H. Lee, M.C. Hsiao, et al, Thermal conductivity and structure of non-covalent functionalized graphene/epoxy composites, Carbon 49 (2011) 5107–5116.
[60] L. Cao, X. Liu, H. Na, Y. Wu, W. Zheng, J. Zhu, How a bio-based epoxy monomer enhanced the properties of diglycidyl ether of bisphenol A (DGEBA)/graphene composites, J. Mater. Chem. A 1 (2013) 5081–5088.
[61] O. Eksik, S.F. Bartolucci, T. Gupta, H. Fard, T. Borca-Tasciuc, N. Koratkar, A novel approach to enhance the thermal conductivity of epoxy nanocomposites using graphene core-shell additives, Carbon 101 (2016) 239–244.